Journal of Materials Chemistry C

Accepted Manuscript

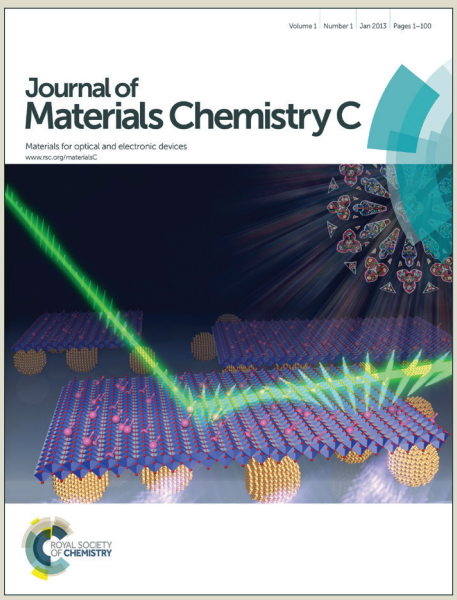

ROYAL SOCIETY OF CHEMISTRY

www.rsc.org/materialsC

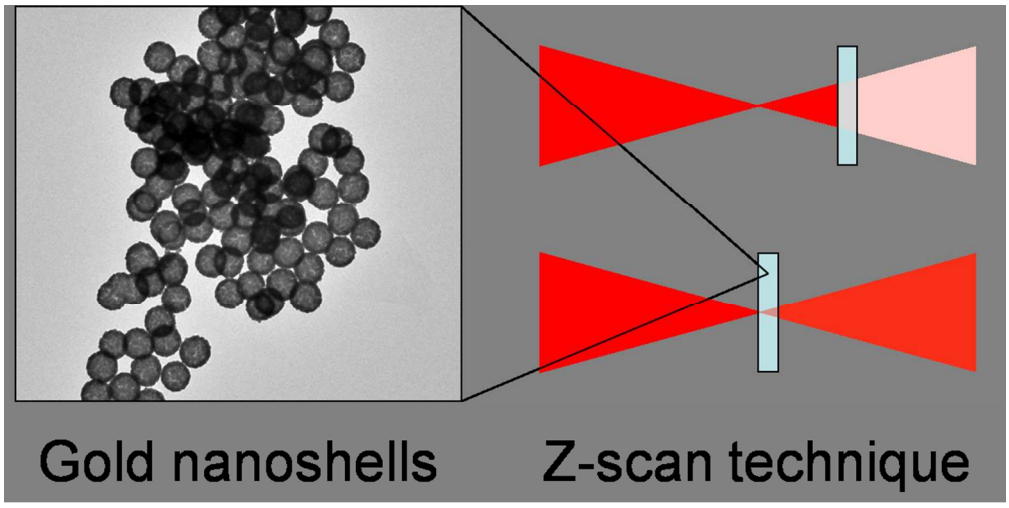

Cite this: DOI: 10.1039/c0xx00000x

www.rsc.org/xxxxxx

ARTICLE TYPE

Shell-thickness-dependent nonlinear optical properties of colloidal gold nanoshells

Marta Gordel,[*ab] Joanna Olesiak-Banska,[*a] Radoslaw Kolkowski,[ac] Katarzyna Matczyszyn,[a] Malcolm Buckle[b] and Marek Samoc[a]

Received (in XXX, XXX) Xth XXXXXXXXX 20XX, Accepted Xth XXXXXXXXX 20XX
DOI: 10.1039/b000000x

Third-order nonlinear optical properties of gold nanoshells of different thickness were investigated over a broad wavelength range (530 - 1200 nm) by the Z-scan technique using femtosecond laser pulses. Nonlinear absorption of the nanoshells is dominated by strong absorption saturation phenomena. The reciprocals of the relevant saturation intensities are the highest at the maxima of one-photon absorption (1PA) bands for all the studied nanoshells but the scaling with the one-photon extinction coefficients within the relevant absorption bands is rather approximate. The reciprocals of the saturation intensities scaled by the values of the extinction coefficients are also found to decrease with the increase of the shell thickness. This can be attributed mostly to the increase of the contribution of the scattering of NIR light to the total extinction of the solutions. The two-photon absorption (2PA) behavior is found to be dominant only within the shortest wavelength range studied for the gold nanoshells with the thinnest shells which exhibit high 2PA cross-section values, with σ_2 reaching $5.1 \cdot 10^{10}$ GM.

Introduction

Among the various plasmonic species investigated to date for their potential applications in photonics and biophotonics the gold nanoshells (NSs) are an interesting class of metal nanoparticles due to their widely tunable properties Au NSs consisting of a core made of silica, surrounded by a gold shell of controlled thickness are an example of easily obtained species of this kind. The frequency of the plasmonic absorption band, which contains components due to the surface plasmons at both the external surface and the shell-core interface of the hybrid nanoparticle, can be continuously tuned through wavelengths, ranging from the ultraviolet into the near-infrared region of 800 - 1200 nm, where the transparent window of biological tissues is located. The position of this band can be controlled via change of the dimensions of the core radius and the shell thickness. The unique tunability and characteristics of nanoshell optical properties spurred a number of proposals for their applications including: *in vitro* visualization[1], optomechanics[2], sensing[3, 4], drug delivery[5, 6], cancer photothermal therapy[7], surface enhanced Raman and surface enhanced infrared absorption spectroscopies[8, 9].

In addition to the linear optical properties of various types of gold nanoparticles there is also much interest in their third-order nonlinear optical (NLO) properties which may be suitable not only for applications in biophotonics[10, 11] but also for optical recording [12], optical limiting [13], high-speed telecommunication [14]. Despite a large number of papers dealing with NLO effects in gold nanoparticles and clusters (entities too small to exhibit surface plasmon resonance) there is confusion concerning the relative strengths of the various NLO effects observed. Since one-photon absorption is present in wide wavelength ranges, saturation of this absorption is often the main effect seen. On the other hand, even in the ranges of one-photon absorption, multiple photon (mostly two-photon) absorption may still be an important effect since it can lead to upconverted light emission. Depending on the technique used for the determination of the NLO effects (e.g. Z-scan measures the total changes of the absorbance while by detecting the upconverted emission one senses only the two-photon absorption component of the NLO effects) various results have been reported. In the case of both gold nanospheres[15] and small, 15-atom gold clusters[16] two-photon absorption (2PA) was seen, a similar behavior was observed in a transverse surface plasmon resonance (t-SPR) range for gold nanorods, however in a longitudinal surface plasmon (l-SPR) range, at relatively low power irradiation the saturated absorption (SA) is more efficient than 2PA, whereas under high-intensity illumination a reverse saturable absorption (RSA) behavior is observed with the clearly visible dip in the relevant Z-scan curve caused by 2PA [17]. Up to now, only a few results were reported concerning the nonlinear optical properties of NSs using the open aperture Z-scan technique. The measurement carried out with 8 ns laser pulses at 532 nm showed saturation of 1PA of colloidal NSs in aqueous solution [18]. Under irradiation at 806 nm, using a fs laser, it was found that NSs also behaved as saturable absorbers. The level of saturation depended on the NSs size and on the laser pulse energy in the range 120 – 300 nJ[19] , but an asymmetry of the saturation peaks was observed, due to reshaping of the NSs under fs illumination.

Studies performed using low repetition rate, short (femtosecond)

pulses in a wide range of the wavelengths are not common. Because plasmonic nanoparticles absorb in a wide range of wavelengths, the use of low repetition rate and short pulses is mandatory for obtaining information on microscopic processes contributing to the nonlinearity, otherwise the NLO response is dominated by cumulative effects such as thermal nonlinearity, nonlinear scattering due to formation of nanobubbles of gases etc. The main purpose of the current paper was to explore the influence of the nanoparticle geometry on the spectral dependences of NLO parameters, which, as we know from our study of NRs[17] can present a complex picture where saturation of the one-photon response competes with resonant multiphoton absorption. An important issue is that plasmonic nanoparticles show strong nonlinear responses that are interesting for applications.

In this article, we describe the fabrication of stable and highly monodisperse NSs suspensions in water, with a varying degree of gold coverage. We provide a detailed description of the third-order nonlinear optical properties of those NSs, determined with low repetition rate fs laser pulses in a wide range of wavelengths (530-1200 nm), using the open- and closed-aperture Z-scan technique. The NLO properties of the nanoshells are quantified in terms of the two-photon absorption coefficient (α_2), the nonlinear refractive index (n_2), and the saturation intensity for one-photon absorption (I_{sat}), which are extensive quantities (dependent on the concentration of the nanoparticles in the investigated solution), dependent on the composition of the studied nanoshells as well as the two-photon absorption cross-section (σ_2) taken per nanoparticle, which can also be interpreted in terms of the merit factor σ_2/M (where M is the molar mass of the nanoparticle), the quantity suitable for comparisons with other types of nonlinear absorbers. We also discuss factors influencing the magnitude of the saturation intensities quantifying the absorption saturation effects. The present results for the nanoshells as well as those for seed nanoparticles, consisting of a 120 nm silica core decorated with 1.5 nm gold islands attached to the surface are compared with results obtained previously by us for gold nanorods using the same open aperture Z-scan setup [17]. The NPs are stable during laser irradiation and any reshaping like that described in Ref[20] is avoided. We discuss the dependences of the NLO data on the NSs shell thickness, the illumination wavelength and the position of the surface plasmon resonance (SPR) band maximum.

Experimental section

Sample preparation

All chemicals were purchased from Sigma-Aldrich except for 120 nm diameter silica nanoparticles which were bought from nanoComposix. Deionized water (18 MΩ) was provided by a Milli-Q system. The synthesis of gold nanoshells was based on the method described by the Halas group [21, 22]. The procedure takes around one month due to the necessary aging of the seed gold. As first, a 1% wt solution of chloroauric acid trihydrate: gold(III) chloride ($HAuCl_4 \cdot 3H_2O$, 99%) in deionized water was prepared, the solution was stored in dark for at least 10 days before use. Then, THPC colloidal gold suspension[23] composed of: tetrakis(hydroxymethyl) phosphonium chloride (THPC, 80% solution in H_2O), sodium hydroxide (1 M), and gold salt solution was prepared, the solution was used after 14 days. The plating solution was prepared by placing 50 mg of potassium carbonate into 200 mL of water, followed by 3 mL of aged gold salt solution (1% $HAuCl_4$). The solution was stored in a dark cabinet at room temperature, used after 48 h. 120 nm silica nanoparticles were coated with 5-10 monolayers of aminopropyltriethoxysilane (APTES 99.99%), at first 15 mL of silica nanoparticles were diluted to 40 mL with deionized water, in a conical centrifuge tube, and centrifuged at 3000 rcf for 25 min, then resuspended in 40 mL of ethanol. The solution was poured into a plastic bottle, stirred, 300 µL of APTES was injected into the suspension and left for 8 h. After the incubation time the solution was centrifuged twice at 3500 rcf for 25 min, finally resuspended into 20 mL of ethanol. To prepare the seed solution 1.5 - 3 nm gold islands were deposited on silica balls covered by APTES layers as follows: 20 mL of THPC colloidal gold suspension was placed in a container, 500 µL of 1M NaCl solution was added, followed by 400 µL of PC 120. The solution was vortexed overnight, centrifuged twice at 1500 rpm for 20 min, finally resuspended in 10 mL of deionized water, stored in a fridge. All the previously prepared compounds were used in gold nanoshells fabrication, in the following way: 3 mL of the plating solution was poured into each of ten plastic cuvettes, then 220 - 400 µL of the seed solution (previously sonicated for 1 minute) followed by 15 µL of formaldehyde (HCHO, 37%). The solution was shaken vigorously for 2 minutes. The procedure was repeated for different volumes of the seed solution. The extinction spectrum was measured to determine the maxima of plasmon resonance peaks. The final nanoshell bath was scaled up by repeating the above procedure with a larger volume of plating solution, seed solution, and formaldehyde in the selected ratio. It was stirred for 10 min, centrifuged once at 120 rpm for 25 min, and resuspended in 30 mL of deionized water.

Sample characterization

The degree of coverage with gold and the average size of the NSs were estimated based on images obtained with a FEI Tecnai G^2 20 X-TWIN Transmission Electron Microscope. The solutions were dropped onto TEM grids and dried before measurement. Concentrations were estimated after drying and weighing the solutions. The average mass of a single gold island, a seed and a NS were calculated assuming that the density of bulk gold is equal to 19300 kg/m^3 and the density of silica (SiO_2) is equal to 2648 kg/m^3. The absorption spectra of the solutions were determined with a JASCO V-670 spectrophotometer.

Z-scan measurements

We performed the closed- and open-aperture Z-scan measurements using a setup and procedures described elsewhere [17, 24, 25]. Briefly, ~130 fs laser pulses at the repetition rate of 1kHz were supplied by a Quantronix Integra-C regenerative amplifier operating as a 800 nm pump, followed by a Quantronix-Palitra-FS BIBO crystal-based optical parametric amplifier. Wavelengths in the range from 530 to 1200 nm were separated from the Palitra output using polarizing wavelength separators and colour glass filters. The beam was focused by a lens to the focal spot with the

beam waist w_0 = 25 – 60 μm. The calculated intensity at the focus of the setup ranged from 60 to 190 GW/cm^2. The pulse energies that are required are ~ 1 μJ and the average power used is on the order of 1 milliwatt. The reference, open-aperture and closed aperture signals were detected by InGaAs photodiodes, collected by a digital oscilloscope, and transferred to a computer using custom-written LabVIEW software. The Z-scan data obtained on NPs solutions were calibrated against closed aperture measurements on a 4.66 mm thick silica plate [17, 24].

The Z-scan measurements were carried out both on the seed solution ("SEED") (120 nm silica nanospheres, covered by gold islands), and on five solutions of gold nanoshells: "NSs 1", "NSs 2", "NSs 3", "NSs 4", "NSs 5" differing in the degree of coverage of the silica cores with gold shells. The solutions were placed in stoppered 1 mm path length Starna cuvettes. After the NLO measurements the solutions were dried, weighed, and concentrations of the NSs were calculated based on the density of the bulk silica and gold.

Theoretical methods

Absorption and scattering spectra of the NSs were simulated using the finite element method implemented in commercial software COMSOL Multiphysics. The geometry: nanoshell surrounded by spherical PML (perfectly matched layer, $\lambda/2n$-thick and distanced by $\lambda/2n$ from NS surface, n = 1.33) was discretized into finite elements using built-in meshing algorithms, with ensured maximum element size 6-10 nm in the shell and $\lambda/6n$ elsewhere, and minimum element quality >0.08. Maxwell equations with appropriate boundary conditions defining the scattering problem were solved in the frequency domain. Absorption cross-sections were calculated by numerical integration of the resistive heating over the volume of the metal, and the scattering cross-sections were obtained by integration of the scattered electric field over the surface of the far-field transform boundary, following the formulas given by Knight and Halas[26], except that the cross-section magnitudes were not normalized by irradiated nanoparticle surface area. Frequency-dependent optical constants of gold, silica and water were taken from references [27-29], respectively.

Results and discussion

The Z-scan experiment was performed on the colloidal seed solution ("SEED") and five different colloidal solutions of gold nanoshells, "NSs1" with uncompleted shell, where the gold layer thickness is up to 10 nm, and "NSs 2", "NSs 3", "NSs 4", "NSs 5" with shell thicknesses: 13 ± 4 nm, 17.5 ± 2 nm, 20 ± 2.5 nm, 25 ± 7 nm, respectively (some additional data taken for uncoated silica shells are shown in the SI). The corresponding TEM pictures are presented in Fig. 1 and the extinction spectra (normalized to $2.26 \cdot 10^{10}$ nanoparticles/ml) in Fig. 2. As evidenced by the UV-vis spectra taken before and after the experiment the nanoparticles were stable during the Z-scan measurement, thus proving that the light intensities and fluence employed were below the threshold of NSs melting.

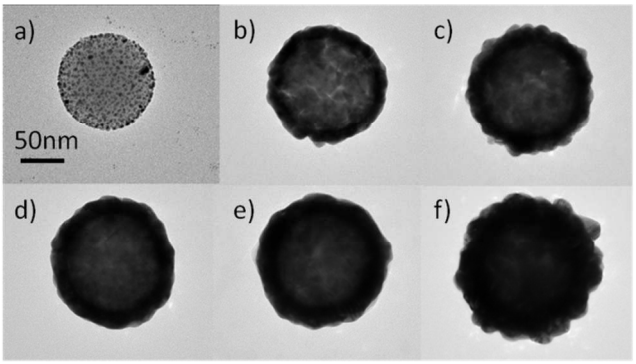

Fig.1 *TEM pictures of selected nanoparticles: a) SEED (120 nm diameter silica core with gold islands), b) uncompleted NSs, where gold thickness is up to 10 nm "NSs1", and NSs with shell thicknesses: c) 13 ± 4 nm "NSs 2", d) 17.5 ± 2 nm "NSs 3", e) 20 ± 2.5 nm "NSs 4", f) 25 ± 7 nm "NSs 5".*

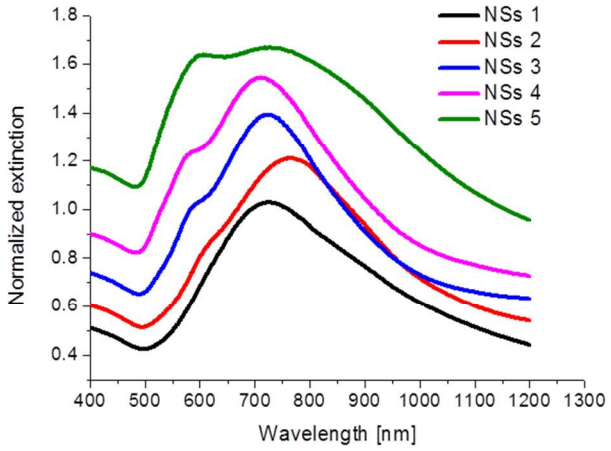

Fig.2 *Extinction spectra normalized to $2.26 \cdot 10^{10}$ nanoparticles/ml for the colloidal solutions of incomplete shell NSs "NSs 1" where gold thickness is up to 10 nm, NSs with shell thickness: 13 ± 4 nm "NSs 2", 17.5 ± 2 nm "NSs 3", 20 ± 2.5 nm "NSs 4", 25 ± 7 nm "NSs 5".*

Representative CA and OA Z-scan traces for "NSs 1" are depicted in Fig. 3. The CA traces were similar for all wavelengths, the beam exhibiting defocusing before and focusing after the focal plane, which is characteristic for positive (self-focusing) refractive nonlinearity. The sample "NSs 1" has the lowest extinction of all tested nanoshells colloidal solutions in the range between 500-560 nm. At the wavelengths 530 nm and 550 nm a dip in the OA trace at the focus is seen, indicating two-photon absorption (2PA) (Fig. 3b). A similar behavior was observed also for the sample "NSs 2". At 600 nm the OA trace is a combination of a peak characteristic for absorption saturation and a decrease of the transmittance at the focus of the beam that indicates the presence of multiphoton absorption (Fig. 3 c). For longer wavelengths only an increase of the transmittance at the focus of the beam was seen (Fig. 3 d) indicating the dominance of saturable absorption over any multiphoton absorption processes.

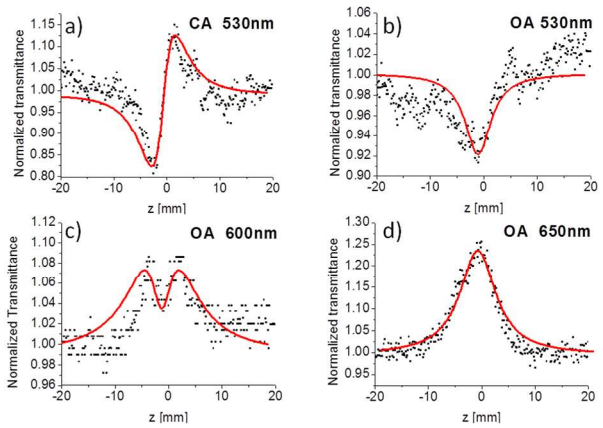

Fig.3 *Representative Z-scan traces of "NSs 1", a) closed-aperture (CA) ; b), c), d) open-aperture (OA). Fitting of OA at 530 nm was performed using an equation describing the 2PA phenomenon, at 600 nm a combination of 2PA and saturation of 1PA was assumed and at 650nm the saturation of 1PA only.*

For quantitative analysis of the results we used equations derived by Sheik-Bahae et at.[25] and their modifications taking into account the saturable absorption behaviour. Nonlinear refraction of the samples was determined from the CA Z-scan traces which were divided by the corresponding OA traces. In all cases the measurements on nanoshell solutions were supplemented by those on cells with the solvent alone and the light intensities were calibrated by CA Z-scans on a silica plate[17]. Similar to Fig.3a, positive nonlinear refraction was measured over the whole wavelength range for all samples. Clearly, the CA signals of the samples that provide the values of n2 for the investigated samples are caused by the changes of the index both in the nanoparticles and in the solvent and at a given concentration of the nanoparticles the relative contributions vary depending on the wavelength. The solvent effect is in most cases dominant but the nanoparticle contribution can be calculated by subtracting the value of the nonlinear phase shift for the solvent from the nonlinear phase shift for the solution during the calculations of the NLO parameters as shown in the example given in the SI. The analysis of the nonlinear absorption was performed by fitting the OA traces as follows. In general, we assumed that the process of absorption of light in the samples can be described by the equation

$$\frac{dI}{dz} = -\alpha_{SA} I - \alpha_2 I^2 \quad (1)$$

which combines two processes: 2PA and saturation of 1PA. In this case the usual one-photon absorption coefficient is substituted with saturable 1PA coefficient α_{SA}. As discussed elsewhere[19, 30], several models of saturable absorption can be considered, in the present case a reasonable agreement with the experiment was obtained for the saturable 1PA coefficient described by the equation typically used for the case of saturation occurring within a homogeneously broadened absorption band [31].

$$\alpha_{SA} = \frac{\alpha_0}{1+\frac{I}{I_{SAT}}} \quad (2)$$

For the "SEED", at all studied wavelengths and for all NSs samples above 600 nm only the saturation of 1PA was observed, giving rise to OA traces with distinct maxima at z = 0. On the other hand, "NSs 1" and "NSs 2", show minima at the focal point for Z-scans taken at 530 nm and 550nm, indicating domination of 2PA. For the other nanoshells samples, the linear absorption in this wavelength range prevents the observation of this phenomenon. All samples show strong absorption saturation effects in the range 600 - 1000 nm. The wavelength dependence of the parameters characterizing the nonlinear absorption is presented in Fig. 4. The σ_2 values for the samples "NSs 1" and "NSs 2" were calculated using the equation:

$$\sigma_2 = \frac{\hbar\omega\alpha_2}{N} \quad (3)$$

where N is the number of nanoparticles in a unit volume.

The two-photon absorption and absorption saturation data in Fig. 4 presented in the same way as in the paper on NLO properties of gold nanorods[17] to facilitate comparisons. Similar to the case of the NRs (and unlike the most commonly studied 2PA processes in organic dyes and many other chromophores), the 2PA observed here is a resonant process, made possible when, under a high photon fluence applied to the system, a hole is created below the Fermi level E_f in the sp band, and then it is filled by a d band electron excited by another photon.

Both NRs and NSs show one-photon absorption extending over the whole visible range. Any multiphoton processes observed in that range must necessarily be treated as competing with one-photon absorption and, since the photons that are used are in resonance with the material excitation, the multiphoton processes are also, by definition, resonant. This does not preclude whether the dominant process is that of simultaneous absorption of two photons or whether there is a time lag between the absorption of the first photon and the second one. Literature data indicate that the dynamics of the process is complex (this is discussed in our paper on nanorods and illustrated with a scheme there)[17]. It is impossible to assess the relative role of processes with different temporal behavior without actual time-resolved (transient absorption) measurements.

It may be noted that the reciprocals of the saturation intensities I_{SAT}^{-1} defined by Eq.(2) have been found to scale approximately with the relevant extinction cross section spectra. Such a scaling might be expected on the basis of consideration of simple saturation kinetics[17]. Therefore, deviations from such a simple correspondence need comment. Unlike the case of relatively small nanorods, the nanoshells studied here are expected to show extinction spectra which may be, to a certain degree, contributed by scattering in addition to the absorption. This is important in the context of NLO studies, since, while the absorption component of the extinction is saturable, the scattering component is not. In fact, there may be a certain influence of light intensity on the efficiency of scattering (due mostly to the intensity-dependent refractive indices at the interfaces of the species contributing to the scattering), but the effects are not supposed to be as dramatic as those due to population changes influencing the absorption.

Clearly, interpretation of the above results requires considering the changes of the contribution of absorption and scattering to the observed extinction, depending on the shell thickness. It was

already reported that the scattering-to-absorption ratio changes significantly with the increase of NSs radius: for NSs having the total radius of 70 nm this ratio was determined to be equal to 0.7, however for NSs with the total radius of 140 nm a significant increase up to 5.3 was observed.[32] In our case the radius varies from around 68 to 92 nm, justifying the need for taking scattering effects into account. In order to do that, we calculated the magnitudes of absorption and scattering cross-sections of all NSs geometries using the COMSOL software (see Theoretical methods section for more details).

One may ask whether an idealized spherical geometry can be used to model NSs having a strongly corrugated surface, such as in Fig.1f. To address these doubts, we performed some additional simulations assuming a more realistic geometry similar to Fig.1f. We have found that even substantial surface roughness (preserving the continuity of the shell) does not change the absorption and scattering spectra, except for a minor red-shift of the resonances. We have not tried to simulate the NLO properties and the influence of the surface roughness on them, which would be very interesting [33, 34], but it is beyond the scope of the present paper. Keeping in mind a number of other factors (such as NS size and shell thickness dispersion), we can carefully apply the results produced by theoretical modeling to interpretation of our experimental data.

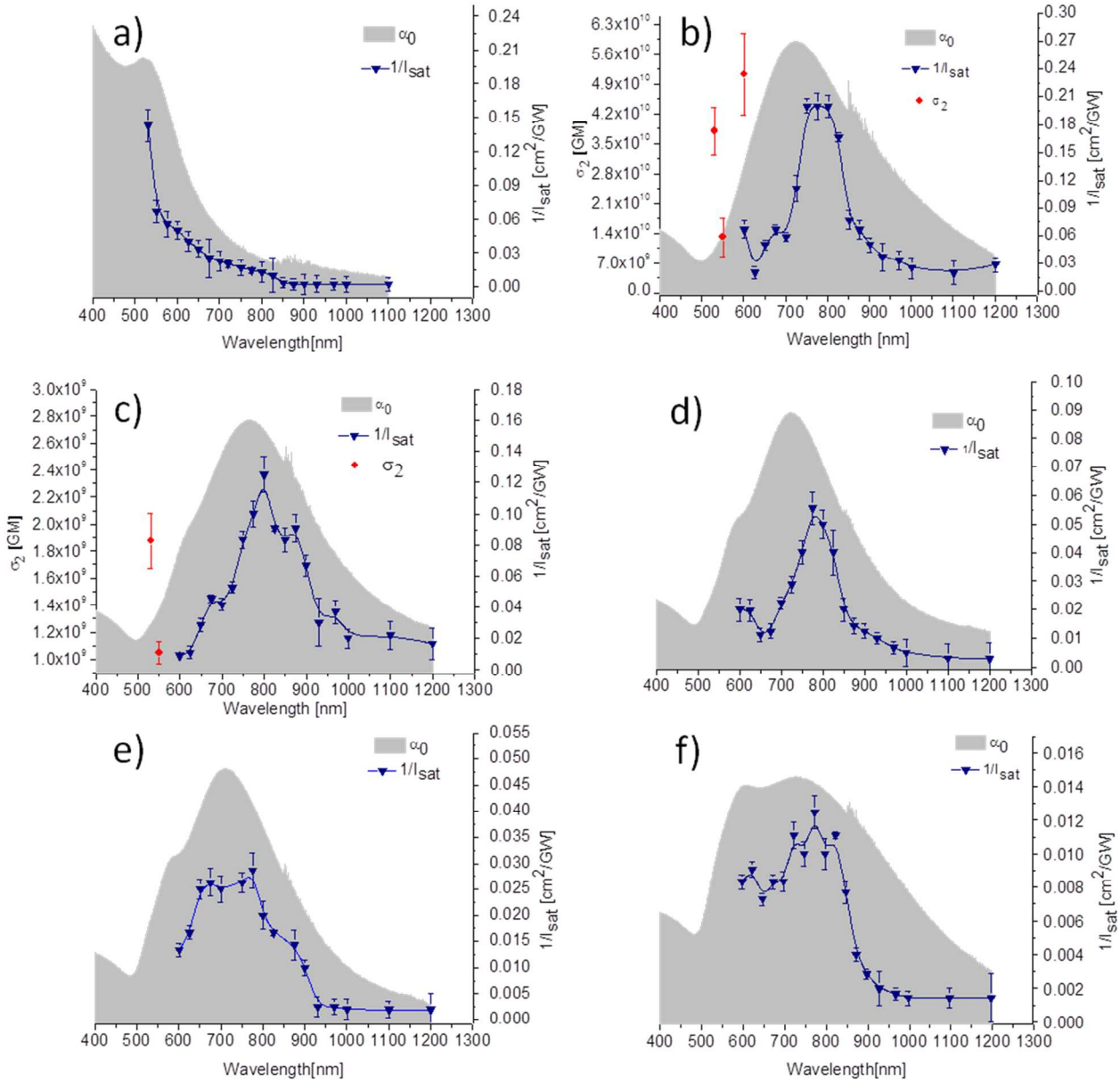

Fig.4 *Graphs showing 2PA cross section (red dots) and the reciprocals of saturation intensity of 1PA (blue triangles, the blue solid line is used to guide its distribution) for: a) SEED, b) "NSs 1", c) "NSs 2", d) "NSs 3", e) "NSs 4", f) "NSs 5". Grey areas represent the 1PA spectra of NSs suspensions.*

The obtained spectral dependences of absorption, scattering and extinction are shown in Fig.5. Two plasmon peaks can be observed in the spectra: a broad peak at lower energy and a sharp peak at higher energy. These modes can be easily identified as

dipolar and quadrupolar resonances, respectively (see insets in Fig.5a). The dipolar mode, which coincides with the spectral maximum of saturation intensity reciprocal for all NSs (700-800 nm), is clearly dominated by scattering, which is almost one order of magnitude greater than absorption. The contribution of absorption in this mode is noticeable in thin nanoshells, but it decreases rapidly with increasing shell thickness (Fig. 5a). This is probably the main cause of the weaker absorption saturation in thicker shells, which is justified by Equation 2 showing a direct relation between the absorption saturation (α_{SA}) and the linear absorption coefficient (α_0). Following this interpretation, one may expect strong absorption saturation in the quadrupolar mode dominated by absorption. In fact, an increased saturation effect can be observed in some NSs (Fig. 4b,d,f). However, the quadrupolar mode appears at higher energy, where the interband transitions leading to 2PA dominate over 1PA saturation processes, making the latter ones difficult to observe.

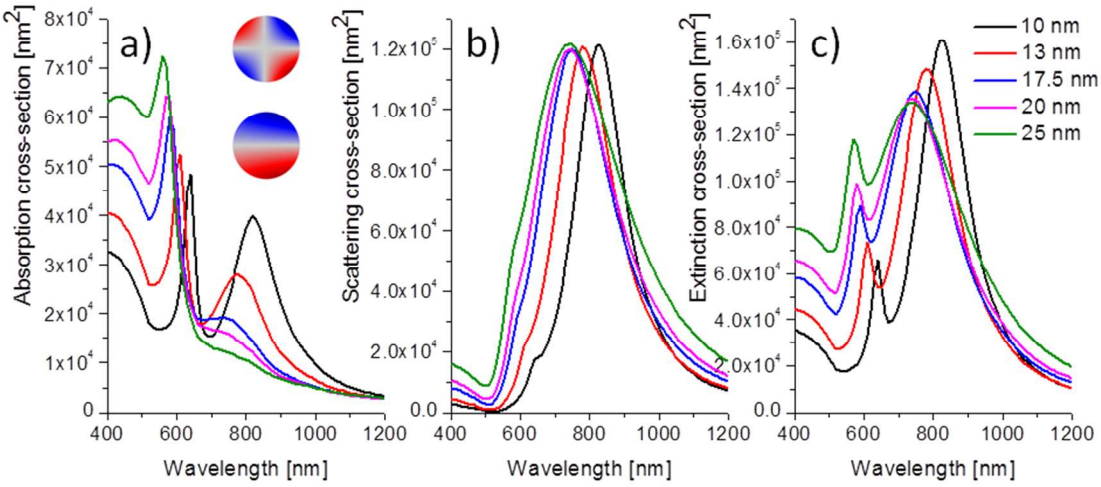

Fig. 5 Optical properties of NSs of various shell thickness, calculated in COMSOL: a) absorption, b) scattering and c) extinction spectra (sum of the previous two). Cross-sections are determined quantitatively in the units of surface area (nm^2), and their magnitudes can be directly compared. Insets in a) show instantaneous surface charge density distribution (red - positive charge, blue - negative charge) corresponding to quadrupolar (upper inset) and dipolar mode (lower inset) at 640 and 820 nm, respectively, of NS with 10 nm shell thickness.

The quantitative data concerning the nonlinear absorption of the nanoshells have to be considered in the context of the nonlinear absorption merit compared with other types of materials. To do that one can employ various merit factors [35, 36]. In the case of two-photon absorption it is useful to normalize the σ_2 value of various species by simply dividing it by the molar mass (M) of the species. Results of these type are listed in Table 1. Since the nanoshells are hybrid species (containing the NLO "inactive" silica core and NLO "active" gold shell), two types of normalization are presented in the table: that referring to the total mass of the nanoparticle and that referring to just the mass of the gold shell. The results do not differ much, though. The nonlinear optical merit of the nanoshells can be compared with those of e.g. gold nanorods.. The value of σ_2/M for gold nanorods (10 nm × 35 nm) at 530 nm is equal to 7.5 (GM·mol/g)[17, 36], while for "NSs 1" it is equal to 1.9 (GM·mol/g) at the same wavelength.

Table 1 *Table shows σ_2 values for studied NSs, their molar mass (M) and the molar mass of the gold covering silica core (M_g). The σ_2 values were normalized to the M and M_g. The last column depicts the reciprocals of saturation intensity divided by the maximum value of α_0 ($(1/I_{sat,\,max})/\alpha_{0,max}$).*

Name of sample	σ_2 [GM] at a given wavelength	M [g/mol]	M_g [g/mol]	σ_2/M	σ_2/M_g	$(1/I_{sat,\,max})$, cm^2/GW	$(1/I_{sat,\,max})/\alpha_{0,max}$
NSs 1	$3.79\cdot10^{10}$ (530 nm)	$2.00\cdot10^{10}$	$1.69\cdot10^{10}$	1.90	2.24	0.21	1.10
	$1.31\cdot10^{10}$ (550 nm)			0.66	0.78		
	$5.12\cdot10^{10}$ (600 nm)			2.56	3.03		
NSs 2	$1.88\cdot10^{10}$ (530nm)	$2.15\cdot10^{10}$	$2.01\cdot10^{10}$	0.87	0.94	0.13	0.93
	$1.05\cdot10^{10}$ (550 nm)			0.49	0.52		
NSs 3	n.a.	$2.38\cdot10^{10}$	$2.23\cdot10^{10}$	n.a.	n.a.	0.06	0.94
NSs 4	n.a.	$3.05\cdot10^{10}$	$2.94\cdot10^{10}$	n.a.	n.a.	0.03	0.38
NSs 5	n.a.	$3.91\cdot10^{10}$	$3.77\cdot10^{10}$	n.a.	n.a.	0.012	0.18

[a]

Cite this: DOI: 10.1039/c0xx00000x

www.rsc.org/xxxxxx

ARTICLE TYPE

Clearly, the nanorods seem to be more efficient, per unit mass of gold, than the nanoshells as two-photon absorbers. On the other hand, due to their huge absolute values of σ_2 (two orders of magnitude larger than those for the considered above nanorods) the nanoshells can still possess an advantage over the much smaller plasmonic nanoparticles with other geometries.

The dominant nonlinear absorption effect with the nanoshells studied here, at the pulse lengths and light intensities used appears to be absorption saturation. We quantified it quoting the values of the reciprocals of the saturation intensities defined by Eq.(2). This quantification is of little use for comparisons between results of experiments carried out under different conditions, including the factor of different sizes of the nanoshells. As mentioned in[17] a simplified model of saturation leads to the conclusion that the saturation intensity may be approximated as $I_{sat}=h\nu\sigma_1^{-1}\tau_1^{-1}$ where σ_1 is the cross section for one-photon absorption and τ_1 is the lifetime of the excited state (assumed to be much shorter than the pulse duration). Results shown in Fig.4 and Table 1 show clearly that the values of I_{sat} increase with the size of the nanoparticles which may be a reflection of the fact that the absorption cross sections of the nanoshells decrease for wavelengths > 600 nm, as the thicknesses of the shells increase. Table 1 lists also the reciprocals of I_{sat} divided by the values of the extinction coefficients of the samples at the maxima of the relevant spectra. It can be seen that the trend of the changes is still preserved, which is understandable, since the experimentally determined extinction (proportional to the sum of the absorption and scattering cross sections) is largely due to scattering while only the absorption cross sections are involved in the saturation.

Conclusions

The NLO results of a range of gold nanoshells with various shell thickness, which we presented here show that gold nanoshells demonstrate a number of features that may be useful in practical applications, especially those involving the absorption saturation. Curiously, the most advantageous combination of the relevant parameters is obtained for the thinnest gold shells. An interesting perspective would be to design a NS with the quadrupolar mode tuned towards NIR, in order to produce a highly efficient saturable absorber in this range of wavelengths.

Acknowledgements

The financial support from NCN Harmonia project UMO-2012/04/M/ST5/00340, a statutory activity subsidy from the Polish Ministry of Science and Higher Education for the Faculty of Chemistry of WUT and the Foundation for Polish Science under the "Welcome" Program is gratefully acknowledged.

Notes and references

[a] *Institute of Physical and Theoretical Chemistry, Wroclaw University of Technology, Wyb. Wyspianskiego 27, 50-370 Wroclaw, Poland email : marta.gordel@pwr.edu.pl, joanna.olesiak@pwr.edu.pl*

[b] *Laboratoire de biologie et pharmacologie appliquée, UMR 8113 CNRS, École normale supérieure de Cachan, 61 Avenue du President Wilson, 94235 Cachan*

[c] *Laboratoire de photonique quantique et moléculaire, École normale supérieure de Cachan, 61, avenue du President Wilson, 94235Cachan, France*

1. R. Bardhan, N. K. Grady and N. J. Halas, *Small*, 2008, 4, 1716-1722.
2. S. R. Sershen, S. L. Westcott, J. L. West and N. J. Halas, *Applied Physics B: Lasers and Optics*, 2001, 73, 379-381.
3. Y. Sun and Y. Xia, *Analytical Chemistry*, 2002, 74, 5297-5305.
4. J. B. Jackson, S. L. Westcott, L. R. Hirsch, J. L. West and N. J. Halas, *Applied Physics Letters*, 2003, 82, 257-259.
5. L. R. Hirsch, N. J. Halas and J. L. West, *Methods in molecular biology (Clifton, N.J.)*, 2005, 303, 101-111.
6. Y. Wu and P. Nordlander, *Journal of Chemical Physics*, 2006, 125.
7. E. S. Day, P. A. Thompson, L. Zhang, N. A. Lewinski, N. Ahmed, R. A. Drezek, S. M. Blaney and J. L. West, *Journal of Neuro-Oncology*, 2011, 104, 55-63.
8. J. Kundu, F. Le, P. Nordlander and N. J. Halas, *Chemical Physics Letters*, 2008, 452, 115-119.
9. F. Le, D. W. Brandl, Y. A. Urzhumov, H. Wang, J. Kundu, N. J. Halas, J. Aizpurua and P. Nordlander, *ACS Nano*, 2008, 2, 707-718.
10. C. Loo, A. Lin, L. Hirsch, M. H. Lee, J. Barton, N. Halas, J. West and R. Drezek, *Technology in Cancer Research and Treatment*, 2004, 3, 33-40.
11. N. Garrett, M. Whiteman and J. Moger, *Optics Express*, 2011, 19, 17563-17574.
12. P. Zijlstra, J. W. M. Chon and M. Gu, *Nature*, 2009, 459, 410-413.
13. M. C. Frare, R. Signorini, V. Weber and R. Bozio, *Proceedings of the SPIE*, 2013, Vol. 8901.
14. M. Février, P. Gogol, G. Barbillon, A. Aassime, R. Mégy, B. Bartenlian, J. M. Lourtioz and B. Dagens, *Optics Express*, 2012, 20, 17402-17410.
15. S. Qu, Y. Gao, X. Jiang, H. Zeng, Y. Song, J. Qiu, C. Zhu and K. Hirao, *Optics Communications*, 2003, 224, 321-327.
16. R. Philip, P. Chantharasupawong, H. Qian, R. Jin and J. Thomas, *Nano Letters*, 2012, 12, 4661-4667.
17. J. Olesiak-Banska, M. Gordel, R. Kolkowski, K. Matczyszyn and M. Samoc, *Journal of Physical Chemistry C*, 2012, 116, 13731-13737.
18. D. J. Wu, X. J. Liu, L. L. Liu and W. P. Qian, *Applied Physics A: Materials Science and Processing*, 2008, 92, 279-282.

19. I. Ros, P. Schiavuta, V. Bello, G. Mattei and R. Bozio, *Physical Chemistry Chemical Physics*, 2010, 12, 13692-13698.
20. M. Gordel, J. Olesiak-Banska, K. Matczyszyn, C. Nogues, M. Buckle and M. Samoc, *Physical Chemistry Chemical Physics*, 2014, 16, 71-78.
21. T. Pham, J. B. Jackson, N. J. Halas and T. R. Lee, *Langmuir*, 2002, 18, 4915-4920.
22. B. E. Brinson, J. B. Lassiter, C. S. Levin, R. Bardhan, N. Mirin and N. J. Halas, *Langmuir*, 2008, 24, 14166-14171.
23. D. G. Duff, A. Baiker and P. P. Edwards, *Langmuir*, 1993, 9, 2301-2309.
24. J. Szeremeta, M. Nyk, D. Wawrzynczyk and M. Samoc, *Nanoscale*, 2012, 5, 2388-2393.
25. M. Sheik-Bahae, A. A. Said, T.-H. Wei, D. J. Hagan and E. W. Van Stryland, *IEEE Journal of Quantum Electronics*, 1990, 26, 760-769.
26. M. W. Knight and N. J. Halas, *New Journal of Physics*, 2008, 10.
27. P. B. Johnson and R. W. Christy, *Physical Review B*, 1972, 6, 4370-4379.
28. G. M. Hale and M. R. Querry, *Applied Optics*, 1973, 12, 555-563.
29. I. H. Malitson, *Journal of the Optical Society of America*, 1965, 55, 1205-1208.
30. M. Samoc, A. Samoc, B. Luther-Davies, H. Reisch and U. Scherf, *Optics Letters*, 1998, 23, 1295-1297.
31. A. E. Siegman, *Lasers* University Science, Mill Valley, Calif, 1986.
32. P. K. Jain, K. S. Lee, I. H. El-Sayed and M. A. El-Sayed, *Journal of Physical Chemistry B*, 2006, 110, 7238-7248.
33. O. Pena-Rodriguez and U. Pal, *Journal of Physical Chemistry C*, 2011, 115, 22271-22275.
34. C. Sauerbeck, M. Haderlein, B. Schurer, B. Braunschweig, W. Peukert and R. N. Klupp Taylor, *ACS Nano*, 2014, 8, 3088-3096.
35. T. Schwich, M. P. Cifuentes, P. A. Gugger, M. Samoc and M. G. Humphrey, *Advanced Materials*, 2011, 23, 1433-1435.
36. M. Samoc, K. Matczyszyn, M. Nyk, J. Olesiak-Banska, D. Wawrzynczyk, P. Hanczyc, J. Szeremeta, M. Wielgus, M. Gordel, L. Mazur, R. Kolkowski, B. Straszak, M. P. Cifuentes and M. G. Humphrey, *Proceedings of the SPIE*, 2012, Vol. 8258.